A Letters Journal Exploring the Frontiers of Physics

September 2010

EPL, **91** (2010) 50002
doi: 10.1209/0295-5075/91/50002

www.epljournal.org

Pinning of vortex rings and vortex networks in excitable systems

Z. A. Jiménez and O. Steinbock[a]

Florida State University, Department of Chemistry and Biochemistry - Tallahassee, FL 32306-4390, USA

received 3 May 2010; accepted in final form 17 August 2010
published online 21 September 2010

PACS 05.45.-a – Nonlinear dynamics and chaos
PACS 82.40.Ck – Pattern formation in reactions with diffusion, flow and heat transfer
PACS 82.40.Qt – Complex chemical systems

Abstract – We investigate the effect of unexcitable obstacles on rotating scroll waves in three-dimensional excitable media. Our experiments use the autocatalytic Belousov-Zhabotinsky reaction and demonstrate that vortex filaments can be pinned to small, spherical obstacles. We find that single pinning sites increase the lifetime of collapsing vortex rings. Lifetimes and accompanying shape changes of the vortex filaments are well described by mean-curvature flow. We also create stationary networks of pinned filaments involving several pinning sites.

Excitable and oscillatory reaction-diffusion systems are known to organize rotating spiral waves of typically constant pitch and frequency. They are found in experimental systems as diverse as the mammalian neocortex, oocytes, catalytic surfaces, corroding steel, and nests of honey bees [1–5]. Over the past two decades systematic research efforts have resulted in a very good understanding of two-dimensional spirals and their response to external fields and gradients [6,7]. Also the pinning of these vortices to unexcitable domains has attracted considerable interest [8–10] which is partly driven by its relevance to cardiology and specifically tachycardia and sudden cardiac death [11,12]. The first, controlled experimental examples of spiral wave pinning were reported for the photosensitive, $Ru(bpy)_3$-catalyzed Belousov-Zhabotinsky (BZ) reaction, where an argon ion laser was used to created photochemically inhibited disks [13]. Other examples include 2D vortex pinning in reacting membrane systems with immobilized catalyst patterns and layers of cultured cardiomyocytes [14,15].

The rotation period of pinned, two-dimensional vortices depends strongly on the perimeter U of the pinning domain and the length of the waves' refractory tail λ_r. For large obstacles ($U \gg \lambda_r$), the spiral tip orbits along the obstacle boundary at a system-specific but constant velocity c_0 yielding a period of $T_0 = U/c_0$. For smaller orbits, (normal) dispersion decreases the wave speed and, hence, causes periods larger than T_0 [13]. Chemical wave rotation around even smaller obstacles ($U \ll \lambda_r$) were studied in microfluidic devices with hundreds of inert obstacles arranged on a square lattice [8]. These conditions induce rotation around obstacle *groups* in which the spiral tip traces complex periodic orbits and the U-dependence of the period follows a devil's staircase. Spiral wave pinning has been also studied for systems with anomalous dispersion which can induce front aggregation in multi-armed spirals [16].

Vortex motion in three-dimensional excitable systems is qualitatively different from its flat counterpart. Foremost, wave rotation occurs around string-like filaments that move with speeds proportional to the local filament curvature. Furthermore, this motion can be affected by changes in the rotation phase ("twist") along the filament [17]. In 2009, we reported the first experimental demonstration of scroll wave pinning [18]. These experiments studied vortex rings attached to torus-shaped obstacles. Such three-dimensional vortex pinning should be possible for wide range of geometric and topological situations including those with striking mismatches between the shape of the filament and the arresting obstacle. This complexity raises a multitude of questions regarding filament dynamics, pinning criteria, forced unpinning, and possible stationary states. To date these questions are widely unanswered. Here, we focus on the pinning of scroll rings to small *spherical* obstacles that increase the local rotation period only slightly. Specifically, we demonstrate vortex pinning involving up to four obstacle units along the filament. We also show that such pinning can prevent the collapse and the annihilation of vortex rings.

Our experiments use the ferroin-catalyzed Belousov-Zhabotinsky (BZ) reaction in which wave propagation is "fueled" by the autocatalytic production and diffusion of

[a]E-mail: steinbck@chem.fsu.edu

bromous acid [19]. This chemical system is a frequently studied experimental model for three-dimensional scroll wave dynamics in excitable systems [20]. To initiate scroll waves in a controlled fashion, we prepare reaction systems in which the lower layer is contained in an agar gel (0.8% w/v), while the upper portion is liquid solution. The thickness of the gel and the liquid layer are 4.0 mm each. The initial concentration of all reactants is the same throughout the two layers: $[H_2SO_4] = 0.16\,\mathrm{mol/L}$, $[NaBrO_3] = 0.04\,\mathrm{mol/L}$, [malonic acid] $= 0.04\,\mathrm{mol/L}$, and $[Fe(phen)_3SO_4] = 0.5\,\mathrm{mmol/L}$. All experiments are carried out at 21.5 °C.

Scroll rings are then created in two steps: 1) With a silver wire we start an expanding spherical wave from an arbitrary point at the gel/liquid interface; 2) several seconds later we briefly mix the liquid phase, which creates a spatially homogeneous top layer and a bowl-shaped wave in the gel portion. The upper rim of this half-sphere curls inwards and nucleates the desired scroll ring. For scroll wave pinning experiments, we introduce chemically inert obstacles into the system. These obstacles are typically spherical glass beads with a radius of 1.0 mm. Prior to the scroll ring initiation, the beads are pressed halfway into the gel.

Wave patterns are detected based on changes in the system's light absorption. Image data are acquired under white light illumination with a CCD camera (equipped with an additive dichroic blue filter) mounted over the system. Accordingly, low and high image intensities correspond to areas in which the employed redox indicator is chemically reduced (excitable) and oxidized (excited or refractory), respectively. We measure the horizontal projection of the scroll wave filaments from image sequences covering about one rotation period of the vortex. The employed method utilizes a characteristic decrease in the absolute change of the local image intensity in and around the filament.

Figures 1(a)–(d) show four consecutive snapshots of a collapsing scroll ring in this chemical system (see also movie file `1beadQT1.mov`). The vortex is pinned to a spherical obstacle which has a profound effect on the scroll ring collapse. In (a) the filament loop is essentially circular with the obstacle at its topmost point. In (b), (c) the filament has become smaller and droplet-shaped. The small dark spots are gas bubbles. The snapshot (d) is recorded shortly before the annihilation of the vortex ring. In contrast to the isotropic shrinkage of free vortex rings [21], the pinned pattern becomes asymmetric and has some qualitative resemblance to a pendant droplet. The cusp of this drop shape is located at the obstacle indicating successful local pinning of the vortex loop. This conclusion is further supported by the space-time plot in fig. 1(e). The latter is constructed from consecutive intensity profiles along a constant line through the obstacle. In the context of the image this line is vertical. The space-time reemphasizes that only the lower pole of the wave emitting filament loop moves while the pinned top stays stationary.

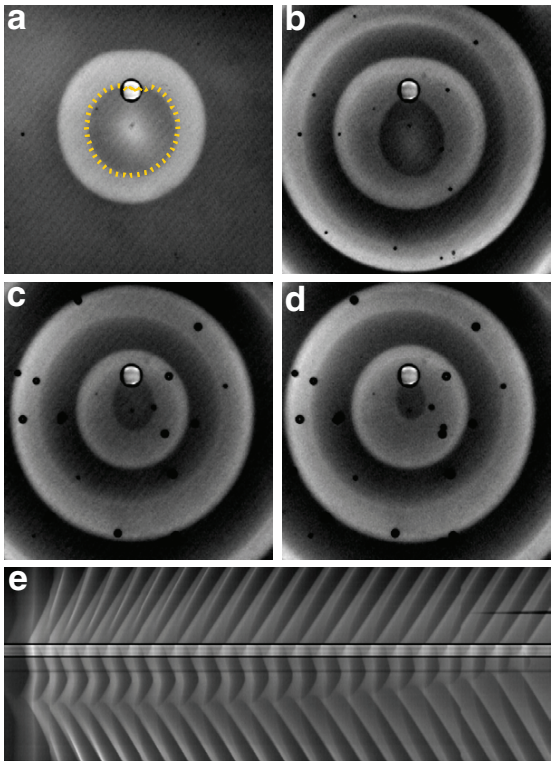

Fig. 1: (Colour on-line) (a)–(d) Consecutive images of a scroll ring in a thick layer of the excitable Belousov-Zhabotinsky reaction. The vortex is pinned to a small spherical obstacle in the upper midsection. Notice that in this projection, the filament loop (see the dotted (yellow) line in (a)) appears as a closed curve emitting inward and outward moving waves in an alternating fashion. This periodic wave emission results from spiral rotation around the filament and is illustrated in the space-time plot (e). Within the context of the figure, the vertical space axis in (e) corresponds to the constant, vertical line in (a)–(d) crossing the obstacle center. Time increases rightwards spanning 9500 s. Images are recorded (a) 560 s, (b) 3600 s, (c) 7440 s and (d) 7960 s after the initiation of the vortex. Field of view (a)–(d): $2.4 \times 2.4\,\mathrm{cm}^2$.

Figure 2 characterizes the key features of the collapse of locally pinned scroll rings. In (a) we show the measured coordinates of a representative filament loop for four different times. A main result concerns the lifetime t_L of the vortex, which for free structures of initial radius R_0 is known to be $t_L = R_0^2/2\alpha$ [21]. In this equation, α is the system-specific filament tension. We find that independent of R_0 the lifetime of a singly pinned vortex ring is increased by a factor of 1.25 ± 0.01 (fig. 2(b)). This effect is accompanied by systematic changes in the filament loop's width w and height h. More precisely, h is here the loop's maximal extension between the pinning obstacle and its lower pole and w is the maximal extension in perpendicular direction. While h, w, and $h + w$ evolve in non-linear fashions, the quantity $(h^2 + w^2)/2$ decreases linearly (fig. 2(c)). We also analyzed the eccentricity of

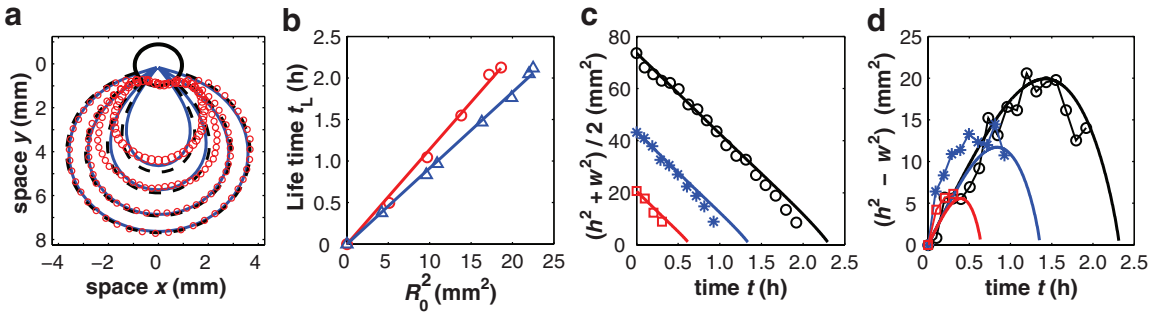

Fig. 2: (Colour on-line) (a) Collapse of a singly pinned scroll wave filament. The obstacle is located around the real-space coordinates (0,0) and shown as a black ring. Open circles (red) are experimental data obtained 900, 2900, 4900, and 6100 s after vortex initiation. (b) Lifetime of singly pinned (red circles) and free (blue triangles) scroll rings as a function of the square of their initial radius. (c) Geometric measure of the pinned filament size as a function of time. The quantities h and w are the filament loops' height and width, respectively. (d) Geometric measure of filament eccentricity as a function of time obtained from the three representative examples in (c). All solid lines in (a)–(d) are obtained by describing the filament motion in terms of mean-curvature flow pinned to a point-shaped site. The dashed curve in (a) illustrates curvature flow with pinning to a circular obstacle and filament termination in normal direction to the obstacle boundary.

the filament loop using the related expression $h^2 - w^2$ (fig. 2(d)), which equals zero for circles. The data show an interesting non-monotonic time dependence of this quantity with a single maximum reached at a time proportional to R_0. Notice that figs. 2(c) and (d) show three representative data sets that differ only in the initial radius of their filament loops. These radii are: 2.26 mm (squares), 3.29 mm (stars), and 4.29 mm (circles). As expected scroll ring annihilation occurs at small but non-zero values of h and w. We suggest that this annihilation point corresponds (at least qualitatively) to the critical radius of wave nucleation [22]. This minor feature is not captured by eqs. (1), (2) and not further studied.

To obtain a better understanding of the main experimental results in fig. 2, we consider the curvature flow model

$$\frac{\mathrm{d}\mathbf{s}}{\mathrm{d}t} = (\alpha\hat{\mathbf{N}} + \beta\hat{\mathbf{B}})\kappa, \qquad (1)$$

which describes the motion of a filament $\mathbf{s}$ in the directions of its unit normal vector $\hat{\mathbf{N}}$ and unit binormal vector $\hat{\mathbf{B}}$. The filament velocity is proportional to the local curvature κ and the proportionality constants α and β are the filament tension and a translational drift coefficient, respectively. Notice that this equation has been derived in earlier studies and is valid for small values of curvature and twist [23,24]. For our BZ system, we find $\alpha = (1.4 \pm 0.1) \times 10^{-5}\,\mathrm{cm}^2/\mathrm{s}$ (see the blue fit in fig. 2(b)) and $\beta \approx 0$. The latter result implies that the filaments in our experiments remain "flat" and do not leave their initial plane. This further simplifies equation (1) to a mean-curvature flow (curve-shrinking) problem. Notice that such curvature flows have diverse applications ranging from quantum field theories to grain boundary dynamics and image processing [25–27].

It is notoriously difficult to find analytical solutions of the seemingly simple equation

$$\mathrm{d}\mathbf{s}/\mathrm{d}t = \alpha\hat{\mathbf{N}}\kappa. \qquad (2)$$

We hence numerically integrate this equation using forward-Euler integration. After each iteration, the curve is reparameterized to yield an essentially constant space resolution of 30 μm. The integration time step is 16 ms. The pinning site is modeled with the Dirichlet boundary condition $(x, y) = (0, 0)$. Notice that this approach reduces the spherical obstacle to a single point.

The results of these simulations are overall in very good agreement with the experimental data in fig. 2. For instance, we find that the lifetime ratio of singly pinned to freely collapsing circles equals 1.28 which is close to the measured value of 1.25. Such characteristic lifetime ratios should exist for all geometrically similar curves with given pinning sites. Interesting examples worthy of further investigation could include families of elliptical filaments with constant (initial) eccentricity and pinning sites.

The linear time dependence of the quantity $(h^2 + w^2)/2$ (fig. 2(c)) is reminiscent but must not be confused with a striking feature of the "free" eq. (2). In the absence of pinning and for closed curves, the enclosed area decreases at a constant rate of $2\pi\alpha$. This result can be readily obtained from the Gauss-Bonnet theorem and has been discussed elsewhere [25,28]. Our finding that singly pinned filament circles recover these dynamics in terms of $(h^2 + w^2)/2$ is not yet understood but might possibly suggest the existence of a more general invariant or a closely related law for pinned curve shrinking. Also the experimentally observed evolution of the loop eccentricity is recovered by the simulations (see fig. 2(d)). We note that the experimental data in (d) have been corrected to compensate for small, initial deviations from perfect

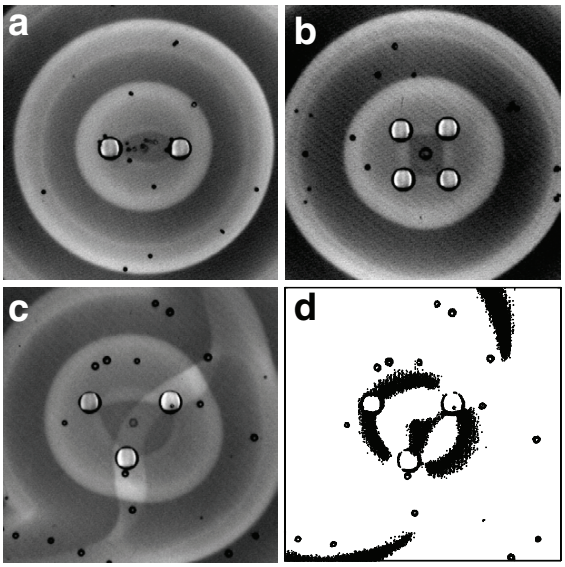

Fig. 3: Scroll rings pinned to (a) two, (b) four, and (c), (d) three spherical obstacles. In (c), a scroll ring is pinned to three obstacles and an additional filament traces an undulating curve across the system. Frame (d) shows a filament reconstruction for the data in (c). Topological constraints suggest that the lower and right obstacles attach to four filaments. Field of view in (a)–(d): $2.4 \times 2.4\,\mathrm{cm}^2$.

circles. The data without this correction (not shown) reveal eccentricity values below the simulated curves but nonetheless match their slopes and overall shape.

Such shape deviations between the curves generated from eq. (2) and the observed filament loops (see *e.g.* innermost curve in fig. 2(a)) could result from our approximation of the pinning obstacle as a single point. We hence studied curvature flow with pinning to the boundary of a disk-shaped region. In these computations, the radius of the disk matches the bead radius in the experiments. The two filament termini evolve under boundary conditions causing their tangential vectors to be (anti)normal to the disk boundary. The results of these computations are shown as dashed curves in fig. 2(a). Deviations between disk- and point-pinning curves are overall small but increase during the later stages of the filament contraction as the disk-pinned filament does not disappear in the center of the disk but at its boundary. More importantly, the simulations still misrepresent the detailed shape of the filament loop. Consequently, additional factors might be relevant such as higher-order curvature terms in eq. (2) or repulsive filament interaction. Lastly we note that these results are the first study of pinned mean-curvature flow.

Scroll wave filaments can also be pinned to more than one obstacle. Figures 3(a), (b) show representative BZ experiments in which initially circular filament loops are pinned to two and four obstacles, respectively. Notice that the emitted waves are nearly circular but have slight elliptical and diamond-shaped deformations in (a) and (b), respectively. A compression-like deformation close to the obstacle can be also discerned in fig. 1(b). We suggest that these deviations are caused by weak twist patterns along the filament. These phase variations are caused by lagging rotation around the obstacle spheres, which are likely to induce tip orbits that are slightly larger than for free rotation. Accordingly wave emission in outward direction is slightly delayed in these regions. Notice that the build-up of twist is limited by diffusion and the overall system dynamics (see *e.g.* [18]). Based on these considerations we predict that larger obstacles should induce more pronounced deformations but we have not further investigated this effect yet.

We find that the collapse of the vortex structures is prevented if its filament is pinned to either three obstacles arranged on the corners of an approximately equilateral triangle (not shown) or four obstacles on a square (fig. 3(b); see also movie file `4beadsQT.mov`). Variations of these three- and four-pin cases as well as larger numbers of obstacles should induce the same stabilization. In all of the latter cases, the filament loop does not remain circular but becomes deformed to a nearly polygonal curve with vertices at the pinning sites. These stationary states do *not* form in the case of two obstacles. The latter situation is qualitatively different as the two filament arches approach the same obstacle-connecting line. Preliminary experimental data suggest that short inter-obstacle distances result in vortex annihilation while large distances cause a seemingly stable lens-shaped filament state (see fig. 3(a)). This finding can be interpreted as evidence of filament repulsion and future analyses of the stationary states might allow the formulation of an effective interaction potential.

All prior examples in this Letter have exactly two filaments terminating on each obstacle. For topological reasons this number has to be even. In addition, the pinned filaments must belong to pairs of counter-rotating vortices (as viewed from the inside of the obstacle) to yield an overall topologically surface charge of zero [29]. The experimental data in figs. 3(c), (d) strongly suggest that the lower and the right obstacle pin four filaments each (see also movie file `3beadsQT_2.mov`). Due to a large wave twist and a certain filament helicity, we did not succeed in resolving the fourth filaments in close vicinity of these two obstacles. This twisting arises from the aforementioned frequency difference between the pinned and the free vortex and is counteracted by the system's diffusion-mediated dynamics. Recent experimental studies showed that this interplay and the resulting twist patterns are well-described by Burgers' equation [18,30]. A direct consequence in our study is that the twist of the freely rotating, long segments is more pronounced than for the shorter obstacle-connecting filaments (fig. 3(c)).

To further evaluate the pinning of multiple filaments to single spherical obstacles, we perform numerical

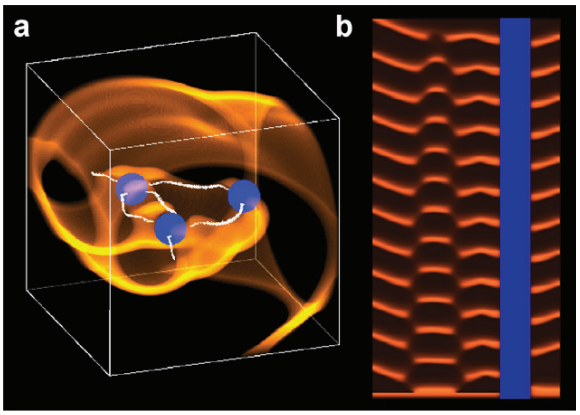

Fig. 4: (Colour on-line) (a) Simulated wave pattern in the Barkley model. Opaque (orange) and fully transparent regions indicate high and low values of the variable v, respectively. The system has three unexcitable, spherical obstacles (blue). Pinned to these obstacles are six filaments (white lines), of which two terminate at the system walls. (b) Space-time plot of the same simulation constructed from the v dynamics along a constant line crossing the right obstacle in (a). Time evolves in upward direction. The wedge-shaped structure corresponds to the decaying double filament in (a).

simulations on the basis of Barkley's excitable reaction-diffusion model [6]

$$\frac{\partial u}{\partial t} = D_u \nabla^2 u + \frac{1}{\epsilon}\left\{u(1-u)\left(u - \frac{v+b}{a}\right)\right\}, \qquad (3)$$

$$\frac{\partial v}{\partial t} = D_v \nabla^2 v + u - v, \qquad (4)$$

where u and v are dimensionless variables. The model parameters are $a = 1.1$, $b = 0.18$, $\epsilon = 0.02$, and $D_u = D_v = 1$. For this choice of identical diffusion coefficients (and in the limit of small curvature and twist), filament motion occurs strictly in normal direction [31]. Spherical obstacles are modeled as unexcitable regions with $u = v = 0$. All scroll waves are initiated by selectively removing regions from a planar wave front. Our simulations use Euler integration with a time step of 6×10^{-3}. The box-shaped system is surrounded by Neumann boundaries and resolved with $300 \times 300 \times 300$ grid points at a constant grid spacing of 0.2.

Figure 4(a) shows a typical example resembling the experimental case in figs. 3(c), (d), which further supports our earlier interpretation. The simulations also reveal that the double-filament connection (see left obstacle pair) is not necessarily stable. For the investigated parameter values, the filament pairs mutually annihilate after finite times that increase with increasing obstacle size and distance. Prior to annihilation, the two filaments move only slightly out of their common initial plane but decrease their distance (fig. 4(b)). Notice that this decrease in inter-filament distance occurs in a nearly linear fashion.

Our numerical studies also revealed that the specific wave field around the filaments strongly depends on the initial conditions. In addition, it is possible that a tetrahedral arrangement of the four filament termini on the obstacle surface might induce greatly enhanced lifetimes of the involved "double bond" and possibly even stable configurations for shorter distances.

In conclusion, we have described the first experimental example of scroll wave pinning to inert spherical obstacles much smaller than the vortex wavelength. The resulting pinned structures have increased lifetimes or evolve into stable, stationary vortex states. The corresponding filament networks obey rigorous topological constraints and organize complex wave fields. Key aspects of scroll wave pinning are well described by mean-curvature flow, thus, providing an ideal platform for future analyses of filament interaction. We believe that our study is also an important stepping stone towards the description of vortex motion in highly heterogeneous media such as neuronal systems and cardiac tissue with unexcitable inclusions.

* * *

This material is based upon work supported by the National Science Foundation under Grant No. 0910657. We thank S. Dutta and A. Kercheval for discussions.

REFERENCES

[1] Huang X. *et al.*, *J. Neurosci.*, **44** (2004) 9897.
[2] Lechleiter J., Girard S., Peralta E. and Clapham D., *Science*, **252** (1991) 123.
[3] Kim M., Bertram M., Pollmann M., von Oertzen A., Mikhailov A. S., Rotermund H. H. and Ertl G., *Science*, **292** (2001) 1357.
[4] Agladze K. and Steinbock O., *J. Phys. Chem. A*, **104** (2000) 9816.
[5] Kastberger G., Schmelzer E. and Kranner I., *PLoS ONE*, **3** (2008) e3141.
[6] Barkley D., *Phys. Rev. Lett.*, **72** (1994) 164.
[7] Mikhailov A. S. and Showalter K., *Phys. Rep.*, **425** (2006) 79.
[8] Ginn B. T. and Steinbock O., *Phys. Rev. Lett*, **93** (2004) 158301.
[9] Tanaka M., Isomura A., Hörning M., Kitahata H., Agladze K. and Yoshikawa K., *Chaos*, **19** (2009) 043114.
[10] Biktashev V. N., Barkley D. and Biktasheva I. V., *Phys. Rev. Lett.*, **104** (2010) 058302.
[11] Clayton R. H., Zhuchkova E. A. and Panfilov A. V., *Prog. Biophys Mol. Biol.*, **90** (2006) 378.
[12] Fenton F. H., Cherry E. M., Hastings H. M. and Evans S. J., *Chaos*, **12** (2002) 852.
[13] Steinbock O. and Muller S. C., *Physica A*, **188** (1992) 61.
[14] Isomura A., Hörning M., Agladze K. and Yoshikawa K., *Phys. Rev. E*, **78** (2008) 066216.

[15] Lim Z. Y., Maskara B., Aguel F., Emokpae R. and Tung L., *Circulation*, **114** (2006) 2113.
[16] Ginn B. T. and Steinbock O., *Phys. Rev. E*, **72** (2005) 046109.
[17] Henry H. and Hakim V., *Phys. Rev. E*, **65** (2002) 046235.
[18] Jiménez Z. A., Marts B. and Steinbock O., *Phys. Rev. Lett.*, **102** (2009) 244101.
[19] Desai R. C. and Kapral R., *Dynamics of Self-organized and Self-assembled Structures* (Cambridge University Press, Cambridge) 2009.
[20] Winfree A. T., *The Geometry of Biological Time* (Springer, New York) 2001.
[21] Bánsági T. and Steinbock O., *Phys. Rev. Lett.*, **97** (2006) 198301.
[22] Keener J. P. and Tyson J. J., *SIAM Rev.*, **34** (1992) 1.
[23] Foerster P., Müller S. C. and Hess B., *Proc. Natl. Acad. Sci. U.S.A.*, **86** (1989) 6831.
[24] Margerit D. and Barkley D., *Chaos*, **12** (2002) 636.
[25] Mullins W. W., *J. Appl. Phys.*, **27** (1956) 900.
[26] Bakas I. and Sourdis C., *J. High Energy Phys.*, **0706** (2007) 057.
[27] Malladi R. and Sethian J. A., *Proc. Natl. Acad. Sci. U.S.A.*, **92** (1995) 7046.
[28] Panfilov A. V., Aliev R. R. and Mushinsky A. V., *Physica D*, **36** (1989) 181.
[29] Pertsov A. M., Wellner M., Vinson M. and Jalife J., *Phys. Rev. Lett.*, **84** (2000) 2738.
[30] Marts B., Bánsági T. jr. and Steinbock O., *EPL*, **83** (2008) 30010.
[31] Alonso S., Kähler R., Mikhailov A. S. and Sagués F., *Phys. Rev. E*, **70** (2004) 056201.